Magnetic structure of hexagonal $YMnO_3$ and $LuMnO_3$ from a microscopic point of view

I. V. Solovyev*
Computational Materials Science Unit, National Institute for Materials Science, 1-2-1 Sengen, Tsukuba, Ibaraki 305-0047, Japan

M. V. Valentyuk† and V. V. Mazurenko
Department of Theoretical Physics and Applied Mathematics, Ural Federal University, Mira str. 19, 620002 Ekaterinburg, Russia
(Received 17 May 2012; published 7 August 2012)

The aim of this work is to establish a basic microscopic picture, which stands behind complex magnetic properties of hexagonal manganites. For these purposes, we consider two characteristic compounds: $YMnO_3$ and $LuMnO_3$, which form different magnetic structures in the ground state ($P6_3cm$ and $P6_3c\underline{m}$, respectively). First, we construct an electronic low-energy model for the Mn $3d$ bands of $YMnO_3$ and $LuMnO_3$, and derive parameters of this model from the first-principles calculations. From the solution of this model, we conclude that, despite strong frustration effects in the hexagonal lattice, the relativistic spin-orbit interaction lifts the degeneracy of the magnetic ground state. Furthermore, the experimentally observed magnetic structures are successfully reproduced by the low-energy model. Then, we analyze this result in terms of interatomic magnetic interactions, which were computed using different types of approximations (starting from the model Hamiltonian as well as directly from the first-principles electronic structure calculations in the local-spin-density approximation). We argue that the main reason why $YMnO_3$ and $LuMnO_3$ tend to form different magnetic structures is related to the behavior of the single-ion anisotropy, which reflects the directional dependence of the lattice distortion: namely, the expansion and contraction of the Mn-trimers, which take place in $YMnO_3$ and $LuMnO_3$, respectively. On the other hand, the magnetic coupling between the planes is controlled by the next-nearest-neighbor interactions, which are less sensitive to the direction of the trimerization. In the $P6_3c\underline{m}$ structure of $YMnO_3$, the Dzyaloshinskii-Moriya interactions lead to the spin canting out of the hexagonal plane, which is additive to the effect of the single-ion anisotropy. Finally, using the Berry-phase formalism, we evaluate the magnetic-state dependence of the ferroelectric polarization, and discuss potential applications of the latter in magnetoelectric switching phenomena.

DOI: 10.1103/PhysRevB.86.054407 PACS number(s): 75.30.−m, 77.55.Nv, 71.15.Mb, 71.10.Fd

I. INTRODUCTION

Hexagonal manganites (the space group $P6_3cm$) are one of canonical examples of multiferroics, which have attracted an enormous attention recently. The coexistence of ferroelectricity and magnetism in these systems provides a unique possibility for manipulating the charges by applying a magnetic field and the spins by applying a voltage. Such a dual nature is crucially important for the construction of new forms of multifunctional devices.[1] To this end, the direct magnetic phase control by static electric field was realized in $HoMnO_3$.[2] The interplay between the ferroelectric activity and the magnetic order was also demonstrated in $YMnO_3$ and $LuMnO_3$ with the measurements of the dielectric constant and the loss tangent. These experiments revealed clear anomalies around the Néel temperature ($T_N = 75$ and 88 K in $YMnO_3$ and $LuMnO_3$, respectively),[3,4] even despite the fact that the ferroelectric transition itself occurred at much higher temperature ($T_C \sim 880$ K).[5] Another spectacular example is the coupling of magnetic and ferroelectric domains, which was visualized in $YMnO_3$ by using the optical second harmonic generation technique.[6] Furthermore, the magnetic transition in $YMnO_3$ and $LuMnO_3$ is accompanied by a distinct change of the atomic positions.[7] Thus the experimental data clearly demonstrates the existence of a strong coupling amongst electric, magnetic, and lattice degrees of freedom in the hexagonal manganites.

The magnetic frustration is one of the key concepts of multiferroic materials, which can assist the inversion symmetry breaking and, in a number of cases, can be even responsible for such a breaking.[8] In this respect, the hexagonal lattice is not an exception and is typically regarded as a playground for studying the magnetic frustration effects. However, it is also the main complication, hampering the theoretical understanding of the multiferroic effect. In this respect, the high-spin state ($S = 2$), realized in the hexagonal manganites, is typically regarded as an "easy case" for the theoretical analysis, where the classical spin fluctuations dominate over the quantum ones. Nevertheless, even in this case, the ground state is expected to be highly degenerate. Different signs of spin fluctuations, apparently originating from this degeneracy, have been observed in the neutron scattering experiments, even below T_N.[9,10] Another evidence of spin fluctuations is the large ratio of the Curie-Weiss temperature (θ_{CW}) to T_N (the so-called frustration parameter), which is about 7 in $YMnO_3$.[9]

The degeneracy can be lifted by lattice distortions and, in this context, plenty of attention is paid to the so-called trimerization instability, inherent to the $P6_3cm$ structure (see Fig. 1).[7,11] However, the trimerization alone does not lift the frustration of isotropic exchange interactions. In this sense, the situation is fundamentally different from the exchange striction effect, which accompanies the formation of the E-type antiferromagnetic (AFM) ordering in the orthorhombic $YMnO_3$ and which lifts the frustration of the nearest-neighbor (NN) interactions.[12] Nevertheless, the trimerization can interplay with the relativistic spin-orbit (SO) coupling and, in this way, give rise to new anisotropic interactions, which can

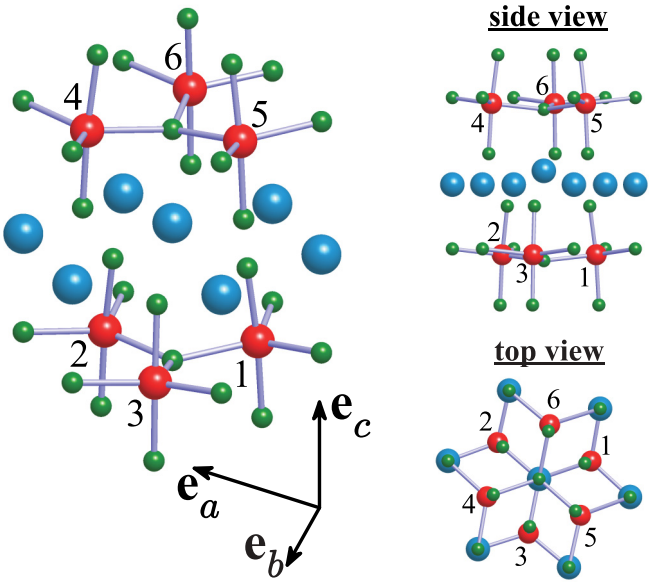

FIG. 1. (Color online) Fragment of the crystal structure of $YMnO_3$. The Y atoms are indicated by the big (blue) spheres, the Mn atoms are indicated by the medium (red) spheres, and the oxygen atoms are indicated by the small (green) spheres. The vectors show the directions of the hexagonal translations. The Mn atoms, forming the trimers in the plane $z = 0$ and $c/2$ are numbered as 1-2-3 and 4-5-6, respectively.

lift the degeneracy and stabilize some individual magnetic structure with the well-defined symmetry. Such structures were detected in the experiments on the neutron diffraction (see Refs. 11, 13, 14) and the optical second harmonic generation (see Ref. 15). In a number of cases (e.g., in $LuMnO_3$), there can be several magnetic structures, coexisting in a narrow temperature range.[15] In short, despite difficulties, there is an enormous experimental progress in the identification of magnetic structures in the hexagonal manganites, resulting from a delicate balance between the lattice distortion, SO interaction, and the frustration effects.

The microscopic understanding of rich magnetic properties of the hexagonal manganites is still rather limited. To begin with, there is no clear microscopic model that would explain the origin of basic magnetic structures in the hexagonal manganites and why different manganites tend to form different magnetic structures. Basically, it is only known how the trimerization affects the isotropic NN exchange interactions.[11] The presence of the single-ion anisotropy and Dzyaloshinskii-Moriya (DM) interactions is, of course, anticipated. However, it is absolutely not clear how all these effects come together to form a rich variety of magnetic structures, realized in the hexagonal manganites.

In this paper, we will try to answer some of these questions. For these purposes, we consider two characteristic manganites: $YMnO_3$ and $LuMnO_3$, which form different magnetic structures in the ground state: $P6_3\underline{c}\underline{m}$ and $P6_3\underline{c}m$, respectively (in the International notations, where each underlined symbol means that given symmetry operation is combined with the time inversion). We will show that this difference can be naturally related to different directions of the trimerization: expansion and contraction of the Mn trimer that takes place in $YMnO_3$ and $LuMnO_3$, respectively. In our study, we start from the first-principles electronic structure calculations in the local-density approximation (LDA). First, we construct a low-energy electronic model, which captures details of the magnetic structure and correctly reproduces the magnetic ground state of $YMnO_3$ and $LuMnO_3$. Then, we analyze these results by further transforming the electronic model into the spin one and elucidating which magnetic interaction is responsible for each detail of the magnetic structure. We will also consider the 'temperature effects', associated with the temperature change of the experimental crystal structure, and show that above T_N it gradually diminishes the anisotropic interactions.

The rest of the paper is organized as follows. All methodological aspects, such as construction of the electronic model and calculation of magnetic interactions, are discussed in Sec. II. Results of solution of the electronic model in the mean-field Hartree-Fock (HF) approximation are presented in Sec. III A. In Sec. III B, we give a detailed analysis of the obtained results in terms of the magnetic interactions, which were computed using different starting points. In Sec. III C, we discuss the magnetic part of the ferroelectric polarization and propose how it can be controlled by switching the magnetic state. Finally, a brief summary of the work is given in Sec. IV.

II. METHOD

Since our goal is the construction of microscopic theory for the magnetic properties of $YMnO_3$ and $LuMnO_3$, we first adopt the low-energy model, which would provide a realistic description for the Mn $3d$ bands of these compounds:

$$\hat{\mathcal{H}} = \sum_{ij}\sum_{\alpha\beta} t_{ij}^{\alpha\beta}\hat{c}_{i\alpha}^{\dagger}\hat{c}_{j\beta} + \frac{1}{2}\sum_{i}\sum_{\alpha\beta\gamma\delta} U_{\alpha\beta\gamma\delta}\hat{c}_{i\alpha}^{\dagger}\hat{c}_{i\gamma}^{\dagger}\hat{c}_{i\beta}\hat{c}_{i\delta}. \quad (1)$$

The model is constructed in the basis of Wannier orbitals for the Mn $3d$ bands, using the input from the first-principles electronic structure calculations in LDA (see Fig. 2). The corresponding procedure was explained in details in the review article (see Ref. 16). Each Wannier orbital is denoted by the Greek symbol, which itself is the combination of the spin ($s = \uparrow$ or $\downarrow$) and orbital ($m = xy$, yz, $3z^2 - r^2$, zx, or $x^2 - y^2$) variables.

All calculations have been performed using experimental parameters of the crystal structure, measured at 10 and 300 K (see Ref. 7, Supplementary Material), i.e., well below and above the magnetic transition point. The experimental space group $P6_3cm$ has 12 symmetry operations, which can be generated by the mirror reflection $x \to -x$, m_x, and the 60°-degree rotation around the z axis, combined with the half of the hexagonal translation, $\{C_z^6|\mathbf{c}/2\}$.

Since the Mn $3d$ bands in hexagonal manganites are well separated from the rest of the spectrum (see Fig. 2), the Wannier basis is complete. In this case, there is one-by-one correspondence between the original LDA band structure and the one, obtained from the one-electron part ($t_{ij}^{\alpha\beta}$) of the model Hamiltonian (1). In this sense, the construction is exact.

The crystal-field splitting, obtained from the diagonalization of the site-diagonal part of $\hat{t}_{ij} = \|t_{ij}^{\alpha\beta}\|$ (without spin-orbit coupling), is very similar for $YMnO_3$ and $LuMnO_3$. For

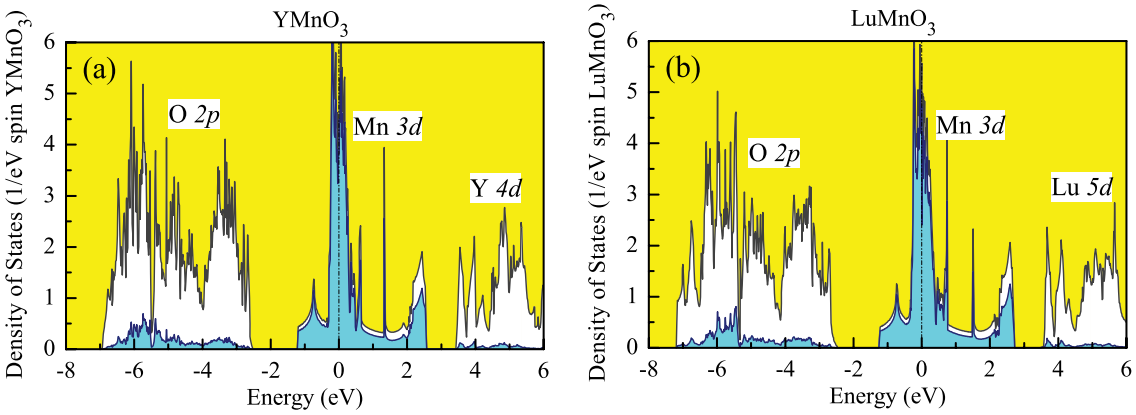

FIG. 2. (Color online) Total and partial LDA densities of states for $YMnO_3$(a) and $LuMnO_3$ (b). The shaded area shows the contributions of the Mn 3*d* states. The positions of the main bands are indicated by symbols. The Fermi level is at zero energy (shown by dot-dashed line).

example, for the 10-K structure, we obtain the following scheme of the atomic energy levels: −0.54, −0.43, −0.29, −0.24, and 1.50 eV in the case of $YMnO_3$, and −0.60, −0.49, −0.25, −0.24, and 1.57 eV in the case of $LuMnO_3$. The 300-K structure yields similar atomic energies. Clearly, the crystal field tends to stabilize four atomic orbitals, which are separated from the fifth one by the energy gap. Such a scheme of the crystal-field splitting is consistent with the formal d^4 configuration of the Mn ions, which is subject to the Jahn-Teller instability. The fifth (unoccupied) orbital is of predominantly $3z^2 - r^2$ symmetry. The off-diagonal elements of $\hat{t}_{ij}$ with respect to the site indices (i and j) stand for the transfer integrals. They are listed in Ref. 17.

The matrix of screened Coulomb interactions $\|U_{\alpha\beta\gamma\delta}\|$ in the Mn 3*d* band was computed in two steps,[16] by applying the constrained LDA and the random-phase approximation (RPA) for the screening. Roughly speaking, the first technique takes into account the screening of the atomic 3*d* orbitals, while the second one—the self-screening by the same 3*d* electrons, which participate in the formation of other bands due to the hybridization.[16] The value of the screened Coulomb interaction U (defined as radial Slater's integral F^0) is about 2.6 eV for all considered systems. The intraatomic exchange (Hund's) coupling $J_{\rm H}$ is about 0.9 eV, which is close to the atomic value. The full matrices of screened Coulomb interactions can be also found in Ref. 17. The obtained value of the screened Coulomb repulsion U is slightly larger than for orthorhombic manganites (about 2.1–2.2 eV),[18] due to the wider energy gap between the O 2*p* and Mn 3*d* bands (see Fig. 2) and, therefore, less efficient RPA screening.[16] It is also important to mention that the parameter U can be estimated by using the more accurate (and more computationally heavy) constrained RPA technique, in the basis of maximally localized Wannier functions.[19] Very recently, this method was applied to $CaMnO_3$.[20] The obtained value of the parameter $U = 2.13$ eV is well consistent with our finding for orthorhombic manganites.[18] Thus we are confident that our estimates for the screened Coulomb interactions are reliable.

After the construction, the model is solved in the HF approximation.[16] This procedure appears to be extremely useful, especially for the search of the magnetic ground state. Typically, in frustrated magnetic systems, we are dealing with the competition of several magnetic interactions of the both relativistic and nonrelativistic origin. Therefore even HF calculations for the relatively simple model (1) can be very time consuming, because they may require tenths of thousands of iterations. In such a situation, the full scale electronic structure calculations are simply unaffordable. Since the degeneracy of the ground state is lifted by the lattice distortion, the HF approximation appears to be a good starting point for the analysis of the equilibrium magnetic properties.[16]

Of course, the model (1) is not perfect, because it does not explicitly include the oxygen band, which can be important for the quantitative analysis of magnetic properties of manganites.[18] Therefore, whenever possible, we check results of our model analysis by comparing them with "all-electron" calculations in the local-spin-density approximation (LSDA). For these purposes, we use the tight-binding linear muffin-tin-orbital method (in the following we will refer to such calculations as "LMTO calculations").[21] Hopefully, in both cases, we can employ the same strategy for calculations of magnetic interactions, which is based on the local force theorem and the Green's function technique. Namely, the isotropic exchange interactions (J_{ij}) can be obtained in the second-order perturbation-theory expansion for the infinitesimal spin rotations,[22] antisymmetric DM interactions ($\mathbf{d}_{ij}$)—by considering mixed type perturbation with respect to the rotations and the relativistic SO coupling,[23–25] and the single-ion anisotropy tensors ($\hat{\tau}_i$)—in the second order with respect to the SO interaction.[26]

The LMTO calculations have been performed for the AFM configuration ↑↓↑↓↑↓, where the arrows stand for the directions of magnetic moments at the sites 1–6 (see Fig. 1 for the notations of atomic positions). The use of the AFM configuration is essential in order to open the band gap in LSDA (about 0.7 eV for $YMnO_3$, which is comparable with the experimental optical gap of 1.3 eV, reported in Ref. 27). The LSDA density of states for the AFM configuration can be found in Ref. 11. Certain inconvenience of working with the AFM ↑↓↑↓↑↓ configuration is that it artificially lowers the $P6_3cm$ symmetry: in this case, the local symmetry can be preserved only around the sites 2 and 5, which will be selected

as the reference points for the analysis of interatomic magnetic interactions.

In our LMTO calculations, we decided to stick to the regular LSDA functional and not to use any corrections for the on-site Coulomb interactions (LSDA+U). On the one hand, such corrections can improve the description for interatomic magnetic interactions (similar to the low-energy model). On the other hand, the use of the LSDA+U functional is always conjugated with some additional uncertainties in the calculations, related to the double-counting problem. Furthermore, the example of orthorhombic $LaMnO_3$ shows that LSDA is indeed a reasonably good starting point for the analysis of interatomic magnetic interactions.[23] Nevertheless, when we compare the LMTO results with the model calculations, we discuss possible consequences of the Coulomb U on the magnetic interactions in the former case.

Due to the hybridization with the oxygen states, which is treated explicitly in the LMTO calculations, the value of spin magnetic moment at the Mn sites is reduced till 3.5 μ_B. Thus some deviation of the local magnetic moment from the ionic value (4 μ_B), which is typically seen in the experiment,[11,13] can be attributed to the covalent mixing. In order to obtain the local magnetic moment in the low-energy model, it is necessary to perform the transformation from the Wannier basis to that of atomic orbitals.[16]

Since for the analysis of the magnetic anisotropy and other effects of the relativistic SO interaction, it is necessary to deal with the total energy differences of the order of several hundredths of microelectron volts, the numerical accuracy of calculations is the very important issue. The key point of our approach is that we deal directly with the total energy differences, responsible for the magnetic properties, and bypass the calculations of large total energies for the whole electron system. This is very important, because the total energy is typically subjected to many sources of error, which are not necessarily related to the magnetism. Therefore the idea is to calculate *directly* the total energy difference, rather than the individual total energies themselves. It is widely used in many applications of the local force theorem,[22] which allow us not only to calculate the total energy difference, but to do it analytically, using the perturbation theory.[22–26] As the result, the numerical accuracy of calculations, based on the local force theorem, is typically very high. The construction of the low-energy model is based on the same idea: it picks up only those electronic states, which are primarily responsible for the magnetism, and abandons the states, which are 'less important'. By doing so, one can get rid of the possible errors, related to the description of these 'less important' states. Of course, which states are important and which are not is sometimes a tricky issue. That is why we should always monitor our model and compare its basic results with all electron calculations (in our case, the LMTO calculations).

Needless to say that, once the model is established, it can be solved very accurately (e.g., using very fine mesh of **k** points, rigid criteria of convergency for the magnetic structure, etc.).[28]

III. RESULTS AND DISCUSSIONS

A. Optimization of magnetic structure

We start with the central result of our work and argue that the low-energy model (1), with the parameters derived from the first-principles electronic structure calculations,[17] successfully reproduces the magnetic ground state of $YMnO_3$ and $LuMnO_3$. The main candidates for the magnetic ground state of $YMnO_3$ and $LuMnO_3$ are shown in Fig. 3 (see also Refs. 13 and 14 for the notations). The unidimensional representations Γ_1, Γ_2, Γ_3, and Γ_4 correspond to the magnetic space groups $P6_3cm$, $P6_3\underline{cm}$, $P\underline{6}_3c\underline{m}$, and $P\underline{6}_3\underline{c}m$, respectively. The directions of the spin magnetic moment, obtained in the HF calculations for the low-energy model, are listed in Table I. In the Γ_1 and Γ_4 configurations, all magnetic moments lie in the xy planes, while in the Γ_2 and Γ_3 configurations, there is also a small canting along the hexagonal z axis. Moreover, the Γ_2 configuration allows for the weak ferromagnetism along z, while in the Γ_3 configuration, the z components of the magnetic

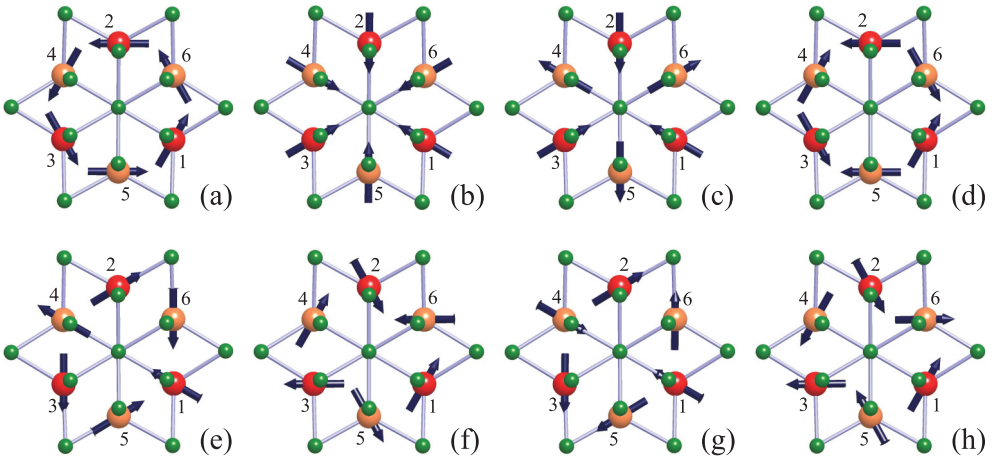

FIG. 3. (Color online) Magnetic structures obtained from the solution of the low-energy model (in the notations of Ref. 13): Γ_1 (a), Γ_2 (b), Γ_3 (c), Γ_4 (d), Γ_5 with $\mathbf{e}_1||[100]$ (e), Γ_5 with $\mathbf{e}_1||[120]$ (f), Γ_6 with $\mathbf{e}_1||[100]$ (g), and Γ_6 with $\mathbf{e}_1||[120]$ (h). The oxygen atoms are indicated by the small green (grey) spheres. The manganese atoms are indicated by the big spheres: the ones located in the $z = 0$ plane are shown by the red (dark) color and the ones in the $z = c/2$ plane are the light orange (grey) color.

TABLE I. The angles α and β, representing the directions $\mathbf{e}_i = (\cos\alpha_i \cos\beta_i, \cos\alpha_i \sin\beta_i, \sin\alpha_i)$ of the spin magnetic moments in the plane $z = 0$, for different magnetic configurations (results of calculations for the low-energy model, using the experimental parameters of the crystal structure at 10 K). The atomic positions are explained in Fig. 1. For the magnetic configurations Γ_1, Γ_2, and Γ_6, the directions of the magnetic moments at the sites 4, 5, and 6 in the plane $z = c/2$ are obtained by the 180° rotations of the vectors $\mathbf{e}_1$, $\mathbf{e}_2$, and $\mathbf{e}_3$ around the z axis. For the magnetic configurations Γ_3, Γ_4, and Γ_5, these 180° rotations should be combined with the time inversion.

Configuration	$YMnO_3$	$LuMnO_3$
Γ_1 and Γ_4	$\alpha_1 = 0, \quad \beta_1 = 60°$ $\alpha_2 = 0, \quad \beta_2 = 180°$ $\alpha_3 = 0, \quad \beta_3 = 300°$	$\alpha_1 = 0, \quad \beta_1 = 60°$ $\alpha_2 = 0, \quad \beta_2 = 180°$ $\alpha_3 = 0, \quad \beta_3 = 300°$
Γ_2 and Γ_3	$\alpha_1 = -0.2°, \quad \beta_1 = 150°$ $\alpha_2 = -0.2°, \quad \beta_2 = 270°$ $\alpha_3 = -0.2°, \quad \beta_3 = 30°$	$\alpha_1 = -0.2°, \quad \beta_1 = 150°$ $\alpha_2 = -0.2°, \quad \beta_2 = 270°$ $\alpha_3 = -0.2°, \quad \beta_3 = 30°$
Γ_5 with $\mathbf{e}_1 \|\|[100]$	$\alpha_1 = -9.6°, \quad \beta_1 = 150°$ $\alpha_2 = 4.8°, \quad \beta_2 = 30.5°$ $\alpha_3 = 4.8°, \quad \beta_3 = 269.5°$	$\alpha_1 = -8.8°, \quad \beta_1 = 150°$ $\alpha_2 = 4.4°, \quad \beta_2 = 30.3°$ $\alpha_3 = 4.4°, \quad \beta_3 = 269.8°$
Γ_5 with $\mathbf{e}_1 \|\|[120]$	$\alpha_1 = 0, \quad \beta_1 = 60°$ $\alpha_2 = -8.3°, \quad \beta_2 = 299.5°$ $\alpha_3 = 8.3°, \quad \beta_3 = 180.5°$	$\alpha_1 = 0, \quad \beta_1 = 60°$ $\alpha_2 = -7.6°, \quad \beta_2 = 299.8°$ $\alpha_3 = 7.6°, \quad \beta_3 = 180.3°$
Γ_6 with $\mathbf{e}_1 \|\|[100]$	$\alpha_1 = -13.4°, \quad \beta_1 = 150°$ $\alpha_2 = 6.6°, \quad \beta_2 = 30.8°$ $\alpha_3 = 6.6°, \quad \beta_3 = 269.2°$	$\alpha_1 = -23.3°, \quad \beta_1 = 150°$ $\alpha_2 = 11.4°, \quad \beta_2 = 30.1°$ $\alpha_3 = 11.4°, \quad \beta_3 = 268.0°$
Γ_6 with $\mathbf{e}_1 \|\|[120]$	$\alpha_1 = 0, \quad \beta_1 = 60°$ $\alpha_2 = -11.5°, \quad \beta_2 = 299.2°$ $\alpha_3 = 11.5°, \quad \beta_3 = 180.8°$	$\alpha_1 = 0, \quad \beta_1 = 60°$ $\alpha_2 = -20.2°, \quad \beta_2 = 297.8°$ $\alpha_3 = 20.2°, \quad \beta_3 = 182.2°$

moments in the planes $z = 0$ and $c/2$ cancel each other. More generally, the configurations Γ_1 (Γ_2) and Γ_4 (Γ_3) differ by the magnetic alignment in the adjacent planes. $\{C_z^6|\mathbf{c}/2\}$ acts as the normal symmetry operation in Γ_1 and Γ_2, which transforms these states to themselves. In the case of the Γ_3 and Γ_4 configurations, $\{C_z^6|\mathbf{c}/2\}$ enters the magnetic symmetry group in the combination with the time-inversion operation $\hat{T}$. It corresponds to the additional flip of the magnetic moments in every second plane of Γ_3 and Γ_4. We have also considered other magnetic configurations with the symmetries Γ_5 and Γ_6, as explained in Ref. 13. However, as it will become clear below, all of them have higher energies.

The total energies of different magnetic configurations are summarized in Table II. Thus the ground state of $YMnO_3$ is Γ_3 ($P\underline{6}_3c\underline{m}$), in agreement with the experiment.[11,15] In $LuMnO_3$, the ground state changes to Γ_4 ($P\underline{6}_3\underline{c}m$), also in agreement with the experiment.[11,15] However, all the states are located in a narrow energy range, which is expected for the frustrated magnetic systems. The lower-symmetry magnetic structure $P\underline{6}_3$, which is typically regarded as another possible candidate for the magnetic ground state of these hexagonal manganites,[11,14,15] appears to be unstable and steadily converges to either $P\underline{6}_3c\underline{m}$ ($YMnO_3$) or $P\underline{6}_3\underline{c}m$ ($LuMnO_3$).

The band gap, obtained for $YMnO_3$ and $LuMnO_3$, is about 2 eV, which is larger than the experimental 1.3 eV.[27] Nevertheless, such an overestimation is quite expectable for the HF approximation: the mean-field HF approach may not be a good starting point for the analysis of the excited-state properties. However, one can expect much better agreement for the ground-state properties: once the degeneracy of the ground state is lifted by the lattice distortion (and/or the relativistic SO interaction), the system can be described reasonably well by the single Slater determinant.[16]

B. Analysis of magnetic interactions

In this section, we clarify results of the HF calculations for the low-energy model and argue that such a good agreement with the experimental data for the magnetic ground state is not surprising and can be anticipated from the behavior of magnetic interactions, which in turn depend on details of the lattice distortions in $YMnO_3$ and $LuMnO_3$. Thus we consider

TABLE II. Total energies of different magnetic configurations as obtained in the Hartree-Fock calculations for the low-energy model. The energies are measured in mircoelectron volt per one formula unit, relative to the most stable configuration. The magnetic configurations are explained in Fig. 3. The calculations for $YMnO_3$ and $LuMnO_3$ have been performed using the experimental crystal structure, measured at 10 and 300 K (indicated in parenthesis).

Configuration	$YMnO_3$ (10 K)	$YMnO_3$ (300 K)	$LuMnO_3$ (10 K)	$LuMnO_3$ (300 K)
Γ_1	0.37	0.20	0.48	0.23
Γ_2	0.16	0.19	0.61	0.32
Γ_3	0	0	0.13	0.10
Γ_4	0.21	0.01	0	0
Γ_5 with $\mathbf{e}_1 \|\|[100]$	0.90	0.76	1.09	1.06
Γ_5 with $\mathbf{e}_1 \|\|[120]$	0.90	0.76	1.09	1.06
Γ_6 with $\mathbf{e}_1 \|\|[100]$	1.06	0.94	1.53	1.27
Γ_6 with $\mathbf{e}_1 \|\|[120]$	1.06	0.94	1.53	1.27

TABLE III. Parameters of isotropic exchange interactions (in meV), calculated in the ferromagnetic state of $YMnO_3$ and $LuMnO_3$. The atomic positions are explained in Fig. 4. Calculations have been performed using the experimental parameters of the crystal structure, measured at 10 K and 300 K (indicated in parenthesis).

Bond	$YMnO_3$ (10 K)	$LuMnO_3$ (10 K)	$YMnO_3$ (300 K)	$LuMnO_3$ (300 K)
2-1	−21.28	−31.81	−23.26	−30.16
2-1′	−26.35	−27.57	−22.67	−27.92
2-4	−0.12	−0.20	−0.13	−0.20
2-5′	−0.19	−0.11	−0.08	−0.10
2-4′	−0.24	−0.31	−0.21	−0.24
2-5	−0.07	−0.16	−0.16	−0.23

the spin model:

$$\hat{\mathcal{H}}_S = -\sum_{\langle ij\rangle} J_{ij}\mathbf{e}_i\mathbf{e}_j + \sum_{\langle ij\rangle} \mathbf{d}_{ij}[\mathbf{e}_i \times \mathbf{e}_j] + \sum_i \mathbf{e}_i\hat{\tau}_i\mathbf{e}_i, \quad (2)$$

which can be obtained by eliminating the electronic degrees of freedom form the more general Hubbard model (1), or directly from the LMTO calculations.[16,22–26] In these notations, $\{J_{ij}\}$ are the isotropic exchange interactions, $\{\mathbf{d}_{ij}\}$ are the antisymmetric DM interactions, $\{\hat{\tau}_i\}$ are the single-ion anisotropy tensors, $\mathbf{e}_i$ stands the *direction* of the spin magnetic moment at the site i, and the summation runs over all *pairs* of atoms $\langle ij\rangle$.

The parameters of isotropic magnetic interactions are listed in Table III, and the atomic positions are explained in Figs. 1 and 4. All NN interactions in the plane xy are AFM. This is reasonable, because the ferromagnetic (FM) coupling in the hexagonal geometry can be stabilized only by virtual hoppings onto the unoccupied $3z^2 - r^2$ orbital, which are relatively small (see Ref. 17). Moreover, the number of orbital paths, available for the virtual hoppings via this particular $3z^2 - r^2$ orbital, is also small. For example, from the orbital decomposition of J_{ij} in our LMTO calculations, we have found that such contributions, involving the $3z^2 - r^2$ orbital,

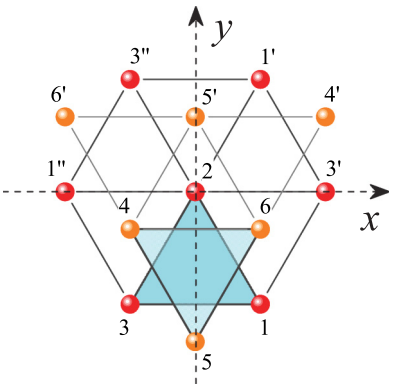

FIG. 4. (Color online) Relative positions of Mn-sites in the hexagonal $P6_3cm$ structure: the atoms located in the plane $z = 0$ are indicated by the red (dark) spheres and the atoms located in the plane $z = c/2$ are indicated by the light orange (grey) spheres. The Mn trimers, which transform to each other by the symmetry operation $\{C_z^6|\mathbf{c}/2\}$, are shaded.

compensates about 30 % of the AFM contributions, involving all other orbitals, except $3z^2 - r^2$.

The symmetry of the $P6_3cm$ lattice is such that there are two types of the NN interactions. The first type takes place in the triangles of atoms 1-2-3 (4-5-6), which are either expanded (the case of $YMnO_3$) or contracted (the case of $LuMnO_3$). The second type takes place in the bonds 2-1′, 2-3′, 2-1″, 2-3″, which are all equivalent. Then, due to the mirror reflection $x \to -x$, the NN bonds 2-4 and 2-6, between adjacent xy planes, are also equivalent and differ from the bond 2-5′. The same situation holds for the next-NN interactions between the planes: there are two equivalent bonds 2-4′ and 2-6′, which differ from the bond 2-5. For the NN interactions, both in and between the planes, there is a clear correlation between the bondlength and the strength of the exchange coupling. For example, in the low-temperature structure of $YMnO_3$, the triangle of atoms 1-2-3 (4-5-6) is *expanded* (for two inequivalent NN bonds 2-1 and 2-1′ in the xy plane, the ratio of the bondlengths is $l_{21'}/l_{21} = 0.961$). Therefore the AFM interaction $J_{21'}$ is stronger than J_{21}.[11] The same tendency holds for the interplane interactions: for two inequivalent NN bonds 2-5′ and 2-4 ($l_{25'}/l_{24} = 0.991$), the AFM interaction $J_{25'}$ is stronger than J_{24}. In $LuMnO_3$, where the triangle of atoms 1-2-3 (4-5-6) is *compressed*, the situation is the opposite: $l_{21'}/l_{21} = 1.016$ and $l_{25'}/l_{24} = 1.003$. Therefore the exchange couplings in the bonds 2-1 and 2-4 are stronger than in the bonds 2-1′ and 2-5′.

The behavior of next-NN interactions between the planes obeys quite different rules. Since the direct transfer integrals are small (see Ref. 17 for details), these interactions are realized by means of the "supersuperexchange" processes via intermediate sites in the pathes $2 \to 6 \to 5$, $2 \to 1 \to 5$, etc., which always include one compressed and one expanded bond. Therefore the simple analysis in terms of the bondlengths is no longer applicable. Instead, we have found that for all considered compounds (and for all considered structures), the AFM interaction in the bond 2-5 appears to be weaker than in the bonds 2-4′ (and in the equivalent to it bond 2-6′). Such a behavior has very important consequences: in a noncollinear structure, it is more favorable energetically to form the FM coupling in the 'weak' bond 2-5 in order to minimize the energy of the AFM interactions in two 'strong' bonds 2-4′ and 2-6′. Particularly, it explains why the magnetic ground state of $YMnO_3$ and $LuMnO_3$ should be Γ_3, Γ_4, or Γ_5, which are characterized by the FM coupling in the bond 2-5, and not Γ_1, Γ_2 or Γ_6, where this coupling is AFM (see Fig. 3). In $LuMnO_3$, this effect is additionally enhanced by the NN interactions between the planes: since AFM interaction in the bond 2-5′ is weaker than in two equivalent bonds 2-4 and 2-6, it is more favorable energetically to form the FM coupling between the sites 2, 5 and 5′ (note that the latter two are connected by the translation). However, in $YMnO_3$, the situation is the opposite and there is a strong competition between the NN and next-NN interactions between the planes. Particularly, it explains a small energy difference between magnetic configurations Γ_3 and Γ_2 (see Table II).

The reliability of the obtained parameters can be checked by calculating θ_{CW}. In the classical Heisenberg model, the latter is given by the formula $\theta_{CW} \approx \sum_i J_{2i}/3k_B$, which yields −562

and −650 K for the 10-K structure of $YMnO_3$ and $LuMnO_3$, respectively. In the quantum case, these values should be additionally multiplied by $(1 + 1/S)$. The structural changes have some effect mainly on $YMnO_3$: if one uses the parameters derived for the 300-K structure, $|\theta_{CW}|$ decreases by 7% (for comparison, similar change of θ_{CW} for $LuMnO_3$ is about 1%). In any case, the obtained values are in a good agreement with experimental data.[4,7,11] The calculations of T_N are not straightforward: due to the quasi-two-dimensional character of isotropic interactions, T_N will be strongly suppressed by thermal fluctuations, as one of the consequences of the Mermin-Wagner theorem.[29] Of course, the molecular-field approximation will overestimate T_N (by factor 4, in comparison with the experiment).

The LMTO calculations yield the following values of the NN interactions in the plane xy (in meV): $(J_{21}, J_{21'}) = (-12.8, -19.6)$, $(-18.0, -17.0)$, $(-15.8, -16.6)$, and $(-17.0, -17.0)$ for $YMnO_3$ (10 K), $LuMnO_3$ (10 K), $YMnO_3$ (300 K), and $LuMnO_3$ (300 K), respectively. Thus all interactions are weaker than in the low-energy model. Nevertheless, this seems reasonable. First, the NN interactions are generally weaker in the AFM ↑↓↑↓↑↓ configuration. This effect was also found in the model calculations, as will become clear below. Second, according to the theory of superexchange interactions in manganites,[30] the ratio of AFM to FM contributions in the NN exchange coupling scales with the value of U as $(U - J_H)/(U + 3J_H)$. Thus $U > J_H$, which was employed in the model analysis, will make this coupling more AFM. Similar tendency was found for interlayer interactions; although LSDA, supplementing the LMTO calculations, somewhat overestimates the FM contributions to the exchange interactions, the modulation of these interactions, caused by the lattice distortion, again favors the formation of the magnetic configurations Γ_3 or Γ_4. For example, in $YMnO_3$ (10 K), the LMTO calculations yield $J_{24} = 0.20$ meV, $J_{25'} = 0.04$ meV, $J_{24'} = -0.14$ meV, and $J_{25} = 0.08$ meV. Therefore these calculations confirm our finding that the experimental coupling between the hexagonal planes is stabilized by the next-NN interactions $J_{25} > J_{24'}$. The NN interactions act in the opposite direction: $J_{25'} < J_{24}$. However, their effect is relatively small (i.e., again, similar to the model).

Let us discuss the behavior of the single-ion anisotropy tensor. Due to the mirror reflection $x \to -x$, the tensor $\hat{\tau}_2$ at the site 2 (see Fig. 4) has the following form:

$$\hat{\tau}_2 = \begin{pmatrix} \tau^{xx} & 0 & 0 \\ 0 & \tau^{yy} & \tau^{yz} \\ 0 & \tau^{zy} & \tau^{zz} \end{pmatrix},$$

where $\tau^{zy} = \tau^{yz}$ and $\tau^{xx} + \tau^{yy} + \tau^{zz} = 0$. Thus the magnetic moments can either lie along the x axis or be perpendicular to it. In the latter case (and if $\tau^{yz} \neq 0$), they are canted out of the hexagonal plane. The anisotropy tensors at other Mn sites can be generated by applying the symmetry operations of the space group $P6_3cm$. The matrix elements of $\hat{\tau}_2$ can be evaluated in the second order of the perturbation theory with respect to the SO interactions.[26] Then, by performing such calculations near the FM state, we obtain the following sets of independent parameters (in meV): $(\tau^{yy}, \tau^{yz}, \tau^{zz}) =$ $(-0.34, -0.12, 0.58)$, $(-0.29, -0.11, 0.58)$, $(-0.25, -0.12, 0.57)$, and $(-0.26, -0.12, 0.57)$ for $YMnO_3$ (10 K), $YMnO_3$ (300 K), $LuMnO_3$ (10 K), and $LuMnO_3$ (300 K), respectively. Since $\tau^{zz} > \tau^{yy}$, all structures that have large z projections of the magnetic moments are energetically unfavorable. Then, by diagonalizing $\hat{\tau}_2$, one can find that the lowest-energy configuration in $LuMnO_3$ is the one where the magnetic moment at the site 2 is parallel to the x axis. The next, canted magnetic configuration, is higher in energy by about 0.05 meV (for the 10-K structure). This situation is reversed in $YMnO_3$, where the lowest energy corresponds to the canted magnetic configuration. The angle α, formed by the magnetic moment and the y axis, is about 7°. In the next configuration, which is higher in energy by about 0.10 meV (for the 10-K structure), the magnetic moment is parallel to the x axis. This energy difference is reduced till 0.01 meV for the 300-K structure. The same behavior was found in the LMTO calculations: for $YMnO_3$, the lowest energy corresponds to the canted magnetic configuration (the canting from the y axis is about 6°). The next configuration, where the magnetic moment is parallel to the x axis, is higher in energy by 0.09 eV for the 10-K structure, and this energy difference further decreases for the 300-K structure.

Thus the change of the ground state from Γ_3 to Γ_4 between $YMnO_3$ and $LuMnO_3$ is related to the behavior of the single-ion anisotropy, which in turns correlates with the distortion of the 1-2-3 triangles (expansion and contraction, respectively). Moreover, due to the 180° rotation around the z axis, which is required in order to transform the site 2 to the site 5 (see Fig. 4), the matrix element τ^{yz} will change sign. Therefore the canting of spins in the planes $z = 0$ and $c/2$ of the Γ_3 structure will act in the opposite directions, and the magnetic moments along the z axis will cancel each other.

The single-ion anisotropy will tend to align the z projections of the magnetic moments ferromagnetically in each of the xy plane. However, this effect will compete with the NN AFM interactions J_{21} and $J_{21'}$. The analytical expression for the spin canting can be obtained by minimizing the energies of single-ion anisotropy and isotropic exchange interactions. Then, by assuming that all neighboring spins in the xy plane form the 120°-structure (as in the case of the Γ_2 and Γ_3 configurations), one can find that

$$\tan 2\alpha = -\frac{2\tau^{yz}}{\tau^{yy} - \tau^{zz} + 3J_{21} + 6J_{21'}}. \qquad (3)$$

Here, the minus-sign corresponds to the situation that is realized in our HF calculations and where $\mathbf{e}_2$ is antiparallel to the y axis (see Fig. 3). Then, for the Γ_3 configuration of $YMnO_3$ (10 K), the canting angle α can be estimated (using both model and LMTO parameters of magnetic interactions) as $\alpha \approx -\tau^{yz}/(3J_{21} + 6J_{21'}) = -0.03°$, which is about seven times smaller than the values obtained in self-consistent HF calculations (see Table I). Nevertheless, there is an additional contribution to the spin canting, caused by the DM interactions.

Parameters of DM interactions between NN sites in the xy plane are listed in Table IV. They were obtained by considering the mixed type of the perturbation theory expansion with respect to the SO interaction and the infinitesimal rotations of the spin magnetic moments.[23] In principle, the parameters $\mathbf{d}_{21'}$ and $\mathbf{d}_{21''}$ are not independent and can be transformed to each other using symmetry operations of the space group

TABLE IV. Parameters of Dzyaloshinskii-Moriya interactions (in meV), calculated in the ferromagnetic states of $YMnO_3$ and $LuMnO_3$. The atomic positions are explained in Fig. 4. Calculations have been performed using the experimental parameters of the crystal structure, measured at 10 and 300 K (indicated in parenthesis).

Bond	$YMnO_3$ (10 K)	$LuMnO_3$ (10 K)	$YMnO_3$ (300 K)	$LuMnO_3$ (300 K)
2-1	(0.01,0.01,0.20)	(0.04,0.02,0.25)	(0.04,0.02,0.17)	(0.07,0.04,0.25)
2-1′	(0.03,−0.02,0.21)	(0.03,−0.02,0.26)	(0.03,−0.01,0.18)	(0.02,−0.01,0.26)
2-1″	(0,0.04,0.21)	(−0.01,0.04,0.26)	(0,0.03,0.18)	(0,0.02,0.26)

$P6_3cm$. However, it is more convenient to consider these two contributions independently. Due to the mirror reflection $x \to -x$, the elements of two *axial* vectors $\mathbf{d}_{23}$ and $\mathbf{d}_{21}$ (see Fig. 4) obey the following rules: $d^x_{23} = d^x_{21}$, $d^y_{23} = -d^y_{21}$, and $d^z_{23} = -d^z_{21}$ (similar situation holds for other NN interactions). Thus they will produce a finite spin canting at the site 2 only if the directions of two other magnetic moments $\mathbf{e}_2$ and $\mathbf{e}_3$ will have an AFM component along x and a FM component along y, i.e., $e^x_3 = -e^x_1$ and $e^y_3 = e^y_1$. Such a situation is realized in the magnetic configurations Γ_2 and Γ_3 (but not in Γ_1 and Γ_4). Then, the magnetic moment at the site 2 will experience the additional rotational force from the sites 1, 1′, and 1″: $\mathbf{f}_{1\to 2} = [\mathbf{d}_{21} \times \mathbf{e}_1] + [\mathbf{d}_{21'} \times \mathbf{e}_1] + [\mathbf{d}_{21''} \times \mathbf{e}_1]$ (note that $\mathbf{e}_1 = \mathbf{e}_{1'} = \mathbf{e}_{1''}$). For the magnetic configurations Γ_2 and Γ_3, the sites of the type "3" will create the same rotational force: $\mathbf{f}_{3\to 2} = \mathbf{f}_{1\to 2}$. However, for the configurations Γ_1 and Γ_4, we will have $\mathbf{f}_{3\to 2} = -\mathbf{f}_{1\to 2}$. Therefore, these two contribution will cancel each other and there will be no spin canting.

These rotational forces should be incorporated in the expression (3) for the spin canting, which yields $\alpha \approx -(\tau^{yz} + f^z_{1\to 2})/(3J_{21} + 6J_{21'}) = -0.04^\circ$. This angle is still smaller than $\alpha \sim -0.21^\circ$, obtained in the HF calculations for the Γ_3 configuration (see Table I). Nevertheless, it should be noted that all the parameters of the spin Hamiltonian (2) were evaluated using perturbation theory expansion near the collinear FM state, which is very far from the ground-state configuration Γ_3. Thus it is interesting to check the effect of the magnetic-state dependence of the parameters of the spin Hamiltonian (2). Indeed, some parameters of the spin Hamiltonian (2) appear to be sensitive to the state in which they are calculated. This can be seen by considering the collinear AFM ↑↓↑↓↑↓ state, where the arrows stand for the directions of magnetic moments at the sites 1–6. In this case, the DM interactions involving the site 2, which is AFM coupled with all NN spins in the xy plane, become (in meV): $\mathbf{d}_{21} = (0.01,0.03,0.01)$, $\mathbf{d}_{21'} = (0.04,0,0)$, and $\mathbf{d}_{21''} = (-0.01,0.05,0.01)$. Then, corresponding rotational force $f^z_{1\to 2}$ will be about two times larger than in the FM state. Meanwhile, the parameters of isotropic exchange interactions J_{21} and $J_{21'}$ decrease by about 15%. These factors will additionally increase $|\alpha|$, but not significantly.

Furthermore, the HF potential for the low-energy model (1) is orbitally dependent. In this case, the local force theorem is no longer valid.[22] Therefore the total energy change due to the SO interaction can be replaced only approximately by the change of the single-particle energies of the HF method. For the single-ion anisotropy, the situation was discussed in Appendix B of Ref. 26. Presumably, this is the main reason, explaining the quantitative difference between results of the electronic and spin model. These are typical uncertainties, supplementing the construction and analysis of the spin model (2).

Nevertheless, the local force theorem is valid within LSDA. Therefore it is interesting to estimate the spin canting in the LMTO calculations, which are based on the LSDA functional. In this case, all DM interactions become larger. For example, for $YMnO_3$ (10 K) we have obtained the following parameters (in meV): $\mathbf{d}_{21} = (-0.01,0.14,-0.20)$, $\mathbf{d}_{21'} = (-0.16,0.04,-0.12)$, and $\mathbf{d}_{21''} = (0.06,0.18,-0.26)$. Then, by combining them with corresponding parameters of the single-ion anisotropy $\tau^{yz} = -0.078$ meV and isotropic exchange interactions J_{21} and $J_{21'}$, which are listed above, we obtain the canting angle $\alpha = -0.12^\circ$. Thus it is interesting that LSDA, despite its limitation, provides the best starting point for the analysis of the spin canting via the perturbation-theory expansion for the spin-orbit interaction, due to validity of the local force theorem. Similar situation was found for the orthorhombic $LaMnO_3$.[23]

Thus although derivation of parameters of spin model (2) may differ in details, this analysis provides a clear microscopic basis for understanding the main difference between $YMnO_3$ and $LuMnO_3$: why the former tends to form the canted noncollinear magnetic structure Γ_3, while the latter forms the planar structure Γ_4.

C. Magnetic contribution to ferroelectric polarization

Finally, we would like to comment on the behavior of the electronic polarization $\mathbf{P}||\mathbf{c}$. It was calculated within the Berry-phase formalism,[31] which was adopted for the model calculations.[8] In this analysis, we use the mesh of the $54 \times 54 \times 30$ $\mathbf{k}$ points in the first Brillouin zone.

Of course, the ferroelectric activity in $YMnO_3$ and $LuMnO_3$ is primarily caused by structural effects. For example, in $YMnO_3$, the ferroelectric transition occurs at about $T_C = 880$ K,[5] which is much higher than $T_N = 75$ K.[7] This fact was also confirmed by the first-principles calculations.[32] Another appealing evidence is that the ferroelectric domains in $YMnO_3$ always coincide with the structural ones.[5] Nevertheless, beside this structural deformation, we have found that there is a substantial magnetic contribution to $\mathbf{P}||\mathbf{c}$. More specifically, all the magnetic configurations can be divided in two groups. The first one includes Γ_1, Γ_2, and Γ_6, where the magnetic moments in the planes $z = 0$ and $c/2$ can be transformed to each other by the simple rotations. The second group includes Γ_3, Γ_4, and Γ_5, where these rotations should be additionally combined with the time inversion. According to our finding, the states in each group are characterized by nearly equal values of $\mathbf{P}||\mathbf{c}$. However, the transition from one group of

states to another would cause a finite jump of the electronic polarization. Thus, in principle, the value of the ferroelectric polarization can be controlled by changing the magnetic state (and vice versa). In this sense, the most promising candidate is $YMnO_3$, where the ground state (Γ_3) and the first excited state (Γ_2) belong to different groups. The energy difference ΔE between these two configurations is about 0.16 meV (see Table II). Then, the change of the ferroelectric polarization, associated with the change of the magnetic state $\Gamma_3 \rightarrow \Gamma_2$, can be estimated as $\Delta \mathbf{P}||\mathbf{c} = -120\ \mu C/m^2$. The practical realization of such a switching phenomenon would be probably interesting, although it is not immediately clear, which external interaction could be used in order to switch the magnetic state. Formally speaking, the magnetic configuration Γ_2 could be stabilized by the external electric field $\mathbf{E}||\mathbf{c}$, which couples to $\Delta \mathbf{P}$ and results in the additional energy gain $-\Delta \mathbf{PE}$. Alternatively, one could exploit the fact that Γ_2 allows for a weak ferromagnetism along z (while Γ_3 does not) and, therefore, could be also stabilized by the interaction with the external magnetic field, $-\Delta \mathbf{MB}$, which couples to the net magnetic moment $\Delta \mathbf{M}$ ($\sim -0.01\mu_B$ per Mn site). However, in order to overcome the total energy difference ΔE, this would require unrealistically large values of $\mathbf{E}$ and $\mathbf{B}$, which cannot be realized in practice. Therefore one should explore alternative possibilities. For example, from the viewpoint of microscopic interactions, one could use the competition of the NN and next-NN interactions between adjacent xy planes, which in the case of $YMnO_3$ act in the *opposite* direction (see discussions above). The Γ_3 configuration is stabilized by the next-NN interactions. However, if one could find such macroscopic conditions, which would shift this balance in the favor of the NN interactions, one could switch the magnetic structure $\Gamma_3 \rightarrow \Gamma_2$ and, therefore, the ferroelectric polarization. Another possibility is, of course, to exploit the magnetism of the rare-earth ions, which can act similar to the external $\mathbf{B}$, but produces much stronger effect on the Mn sublattice. Such a magnetic phase control was indeed realized experimentally in the series of hexagonal manganites with the magnetic rare-earth sublattices.[2,33]

IV. SUMMARY

Using results of first-principles electronic structure calculations, we have established the low-energy model, which is able to deal with basic magnetic properties of the hexagonal manganites. This Hubbard-type model describes the behavior of the Mn $3d$ bands, being subjected to the lattice deformation and the on-site electron-electron interactions. All the parameters of such model, obtained for $YMnO_3$ and $LuMnO_3$, are summarized in Ref. 17.

Then, the model was solved in the mean-field HF approximation, by considering all possible noncollinear magnetic structures with different symmetries. Since the magnetic frustration is lifted by the relativistic SO interaction, the HF approach provides a good starting point for the analysis of the ground-state properties of these compounds. It successfully reproduces the experimental change of the magnetic structure of $YMnO_3$ and $LuMnO_3$ from $P\underline{6}_3c\underline{m}$ to $P\underline{6}_3\underline{c}m$.

In order to clarify the microscopic origin of this change, we have further transformed the electronic model into the spin one and discussed the same trend in terms of differences in the behavior of isotropic and anisotropic magnetic interactions. We have found that the main reason why $YMnO_3$ and $LuMnO_3$ tend to form different magnetic structure is related to the behavior of the single-ion anisotropy. The latter is coupled to the trimerization distortion in the hexagonal plane, which has different directions in the case of $YMnO_3$ and $LuMnO_3$ (expansion and construction of the Mn trimers, respectively). On the other hand, the interplane coupling is controlled by the next-NN isotropic exchange interactions, which are less sensitive to the direction of the trimerization. The spin canting in the $P\underline{6}_3c\underline{m}$ structure of $YMnO_3$ is a joint effect of the single-ion anisotropy and Dzyaloshinskii-Moriya interactions, which act in the same direction. As the trimerization distortion decreases with the temperature, all anisotropic interactions also decrease, thus reviving the magnetic frustration and the degeneracy of the magnetic state.

Finally, using the Berry-phase formalism, we have estimated the magnetic contribution to the ferroelectric polarization and discussed how it can be controlled by changing the magnetic structure of $YMnO_3$.

ACKNOWLEDGMENTS

The work of M.V.V. and V.V.M. is supported by the grant program of President of Russian Federation MK-406.2011.2, the scientific program "Development of scientific potential of Universities", RFFI 12-02-90810, and the grant of the Ministry of education and science of Russia No. 12.740.11.0026.

*SOLOVYEV.Igor@nims.go.jp

†Temporarily at Institute of Theoretical Physics, University of Hamburg, Jungiusstrasse 9, 20355 Hamburg, Germany.

[1] S.-W. Cheong and M. Mostovoy, Nat. Mater. **6**, 13 (2007).

[2] Th. Lottermoser, Th. Lonkai, U. Amann, D. Hohlwein, J. Ihringer, and M. Fiebig, Nature (London) **430**, 541 (2004).

[3] Z. J. Huang, Y. Cao, Y. Y. Sun, Y. Y. Xue, and C. W. Chu, Phys. Rev. B **56**, 2623 (1997).

[4] T. Katsufuji, S. Mori, M. Masaki, Y. Moritomo, N. Yamamoto, and H. Takagi, Phys. Rev. B **64**, 104419 (2001).

[5] T. Choi, Y. Horibe, H. T. Yi, Y. J. Choi, W. Wu, and S.-W. Cheong, Nat. Mater. **9**, 253 (2010).

[6] M. Fiebig, Th. Lottermoser, D. Fröhlich, A. V. Goltsev, and R. V. Pisarev, Nature (London) **419**, 818 (2002).

[7] S. Lee, A. Pirogov, M. Kang, K.-H. Jang, M. Yonemura, T. Kamiyama, S.-W. Cheong, F. Gozzo, N. Shin, H. Kimura, Y. Noda, and J.-G. Park, Nature (London) **451**, 805 (2008).

[8] I. V. Solovyev and Z. V. Pchelkina, Phys. Rev. B **82**, 094425 (2010); I. V. Solovyev, *ibid.* **83**, 054404 (2011). Note that a prefactor was missing in the previous model calculations of $\mathbf{P}$, and all values

of the electric polarization, reported in these two papers, should be additionally divided roughly by 2.5. This partly resolves the problem of disagreement with the experimental data. The details will be discussed in a separate publication.

[9] J. Park, J.-G. Park, G. S. Jeon, H.-Y. Choi, C. Lee, W. Jo, R. Bewley, K. A. McEwen, and T. G. Perring, Phys. Rev. B **68**, 104426 (2003).

[10] T. J. Sato, S.-H. Lee, T. Katsufuji, M. Masaki, S. Park, J. R. D. Copley, and H. Takagi, Phys. Rev. B **68**, 014432 (2003).

[11] J. Park, S. Lee, M. Kang, K.-H. Jang, C. Lee, S. V. Streltsov, V. V. Mazurenko, M. V. Valentyuk, J. E. Medvedeva, T. Kamiyama, and J.-G. Park, Phys. Rev. B **82**, 054428 (2010).

[12] D. Okuyama, S. Ishiwata, Y. Takahashi, K. Yamauchi, S. Picozzi, K. Sugimoto, H. Sakai, M. Takata, R. Shimano, Y. Taguchi, T. Arima, and Y. Tokura, Phys. Rev. B **84**, 054440 (2011).

[13] A. Muñoz, J. A. Alonso, M. J. Martínez-Lope, M. T. Casáis, J. L. Martínez, and M. T. Fernández-Díaz, Phys. Rev. B **62**, 9498 (2000).

[14] P. J. Brown and T. Chatterji, J. Phys.: Condens. Matter **18**, 10085 (2006).

[15] M. Fiebig, D. Fröhlich, K. Kohn, St. Leute, Th. Lottermoser, V. V. Pavlov, and R. V. Pisarev, Phys. Rev. Lett. **84**, 5620 (2000).

[16] I. V. Solovyev, J. Phys.: Condens. Matter **20**, 293201 (2008).

[17] See Supplemental Material at http://link.aps.org/supplemental/10.1103/PhysRevB.86.054407 for parameters of the crystal field, transfer integrals, and matrices of Coulomb interactions.

[18] I. Solovyev, J. Phys. Soc. Jpn. **78**, 054710 (2009).

[19] T. Miyake and F. Aryasetiawan, Phys. Rev. B **77**, 085122 (2008).

[20] H. Ohnishi, T. Kosugi, T. Miyake, S. Ishibashi, and K. Terakura, Phys. Rev. B **85**, 165128 (2012).

[21] O. K. Andersen, Z. Pawlowska, and O. Jepsen, Phys. Rev. B **34**, 5253 (1986).

[22] A. I. Liechtenstein, M. I. Katsnelson, V. P. Antropov, and V. A. Gubanov, J. Magn. Magn. Mater. **67**, 65 (1987).

[23] I. Solovyev, N. Hamada, and K. Terakura, Phys. Rev. Lett. **76**, 4825 (1996).

[24] V. V. Mazurenko and V. I. Anisimov, Phys. Rev. B **71**, 184434 (2005). Note that this work employed the same strategy for derivation of parameters of DM interactions as in Ref. 23, but different choice of phases in the spin-rotation matrix. Namely, the rotation of spin from $\mathbf{e}^0 = (0,0,1)$ to $\mathbf{e} = (\cos\varphi \sin\theta, \sin\varphi \sin\theta, \cos\theta)$ was described by the following sets of the Euler angles: $(\alpha_I,\beta_I,\gamma_I) = (\varphi,\theta,-\varphi)$ in this work and $(\alpha_{II},\beta_{II},\gamma_{II}) = (\varphi,\theta,0)$ in Ref. 23. The second choice provides more compact expression for DM interactions and allows to get rid of the on-site contribution to the rotational force. Of course, the total force, created by all spins, does not depend on the phase choice.

[25] A. N. Rudenko, V. V. Mazurenko, V. I. Anisimov, and A. I. Lichtenstein, Phys. Rev. B **79**, 144418 (2009).

[26] I. V. Solovyev, P. H. Dederichs, and I. Mertig, Phys. Rev. B **52**, 13419 (1995).

[27] A. M. Kalashnikova and R. V. Pisarev, JETP Lett. **78**, 143 (2003).

[28] In our HF calculations for the low-energy model, we used the mesh of the $12 \times 12 \times 6$ $\mathbf{k}$ points in the first Brillouin zone. In order to monitor the convergency, we calculate the quantity $\epsilon = \left(\sum_{\alpha\beta} \mathcal{V}_{\alpha\beta}^{\text{out}} - \mathcal{V}_{\alpha\beta}^{\text{in}\,2}\right)^{1/2}$, where $\mathcal{V}_{\alpha\beta}$ are the matrix elements of the HF potential, used at the input (in) and obtained as the output (out) of each iteration. The magnetic structure was considered as converged if $\epsilon < 10^{-7}$ Ry.

[29] N. D. Mermin and H. Wagner, Phys. Rev. Lett. **17**, 1133 (1966); **17**, 1307(E) (1966).

[30] K. I. Kugel and D. I. Khomskii, Sov. Phys. Usp. **25**, 231 (1982).

[31] D. Vanderbilt and R. D. King-Smith, Phys. Rev. B **48**, 4442 (1993); R. Resta, J. Phys.: Condens. Matter **22**, 123201 (2010).

[32] B. B. van Aken, T. T. M. Palstra, A. Filippetti, and N. A. Spaldin, Nat. Mater. **3**, 164 (2004).

[33] M. Fiebig, Th. Lottermoser, and R. V. Pisarev, J. Appl. Phys. **93**, 8194 (2003).